

Article

Selective Laser Melting of Inconel 718/TiC Composite: Effect of TiC Particle Size

Vadim Sufiiarov * , Danil Erutin, Evgenii Borisov and Anatoly Popovich

Institute of Mechanical Engineering, Materials, and Transport, Peter the Great St. Petersburg Polytechnic University, 195251 St. Petersburg, Russia

* Correspondence: vadim.spbstu@yandex.ru

Abstract: In this article, we present the results of a study of the effect of TiC particle size on the microstructure and properties of a composite material based on the heat-resistant nickel alloy Inconel 718. Composite materials with the addition of 1% mass of micron- or nano-sized TiC particles were successfully manufactured by selective laser melting. Hot isostatic pressing and heat treatment were applied to manufactured samples. Increasing hardness with the addition of TiC particles by about 20% without dependence on TiC size was determined. The addition of nano-sized TiC leads to a greater increase in strength characteristics at room temperature and elevated temperature of 700 °C in comparison with pure Inconel 718 and the addition of micron-sized TiC particles, but also leads to decreasing elongation.

Keywords: additive manufacturing; superalloy; selective laser melting; Inconel; TiC; mechanical properties; microstructure; composite



Citation: Sufiiarov, V.; Erutin, D.; Borisov, E.; Popovich, A. Selective Laser Melting of Inconel 718/TiC Composite: Effect of TiC Particle Size. *Metals* **2022**, *12*, 1729. <https://doi.org/10.3390/met12101729>

Academic Editor: Baicheng Zhang

Received: 15 September 2022

Accepted: 13 October 2022

Published: 15 October 2022

Publisher's Note: MDPI stays neutral with regard to jurisdictional claims in published maps and institutional affiliations.



Copyright: © 2022 by the authors. Licensee MDPI, Basel, Switzerland. This article is an open access article distributed under the terms and conditions of the Creative Commons Attribution (CC BY) license (<https://creativecommons.org/licenses/by/4.0/>).

1. Introduction

Nickel-based superalloys can be characterized as the most suitable materials for loaded details, whose work implies high environment temperatures [1,2]. Inconel 718 is the remarkable representative of this category of materials, and it is used in nuclear reactors, gas turbines and other parts susceptible to creep and oxidation [3]. The main feature of this composition is precipitation hardening, which can be achieved using heat treatment [4–6].

The geometric complexity of the needed workpieces makes additive manufacturing technologies, such as selective laser melting, convenient for mass production of various details [7–10]. Selective laser melting (SLM) is the additive manufacturing process by layer-by-layer melting of a 20–100 µm thick powder layer of material using a laser [11,12]. This process allows a fine microstructure to be obtained but does not allow obtaining dense metal. This circumstance makes it essential to use hot isostatic pressing for a blank (as-built) SLM sample to improve its mechanical properties.

Improving the mechanical properties of superalloys is a priority in the production of high-temperature details. For the best mechanical performance, it is vital to use the two-step heat treatment comprising solution annealing and aging, which facilitates the formation of micro-particles of intermetallic compounds in the matrix [13–17]. Additional mechanical reinforcement can be achieved by including some ceramic and carbide particles into the Inconel 718 matrix, such as TiC, WC [18–21], BN [22] and TiB₂ [23]. It is recognized that particle distribution in a composite constituting a particulate-reinforced composite [24–27], independent of the material particles involved (i.e., hard and soft particles [26]), has an important impact on the resulting properties [24,27]. Among these materials, TiC had the most significant effect on the microhardness and wear-resistance of the Ni-based alloy [28], and it is important to understand how the addition of TiC particles to Inconel 718 powder will affect its properties after SLM.

The authors of [29] studied the effect of TiC content in Inconel 718 powder on the microstructure and mechanical properties of selective laser-melted Inconel 718/TiC composites. The researchers prepared powders of Inconel 718 with 0.25%, 0.5%, 0.75% and 1% nano-TiC particles and found that the selective laser-melted sample with 1% nano-TiC has a dendritic cell size of approximately 0.3 μm as opposed to the blank selective laser-melted Inconel 718, with a cell size of 2–3 μm . In terms of mechanical properties, the sample with 1% nano-TiC has an optimal complex of strength and plasticity among studied nano-TiC mass percentages. Another group of researchers [30] investigated the effect of solid solution and aging heat treatment on the microstructure and mechanical properties of Inconel 718/nano-TiC composites obtained with selective laser melting, and their data attest that the most effective solution annealing temperatures were 1020 $^{\circ}\text{C}$ and 1100 $^{\circ}\text{C}$. Heat treatment using these temperatures increased the tensile strength of the samples by approximately 20% as compared to untreated samples. The data obtained by these research groups form the basis of the present work, which contains high-temperature strength and elongation data in contrast with other papers.

The aim of this work was to investigate the effect of adding TiC particles of different sizes on the microstructure and room- and high-temperature mechanical properties of selective laser-melted Inconel 718 alloys in blank SLM conditions and after hot isostatic pressing and two-step heat treatment.

2. Materials and Methods

Initial powders of Inconel 718 (MetcoAdd 718C, Oerlicon, Pfäffikon, Switzerland), micron-sized TiC (polyhedral particles with mean size of 17.1 μm) and nano-sized TiC (agglomerations of spherical particles with mean size of 60 nm) (Sigma-Aldrich, St. Louis, MO, USA) were used in the present study (Figure 1). Chemical compositions of the TiC powders are presented in Table 1.

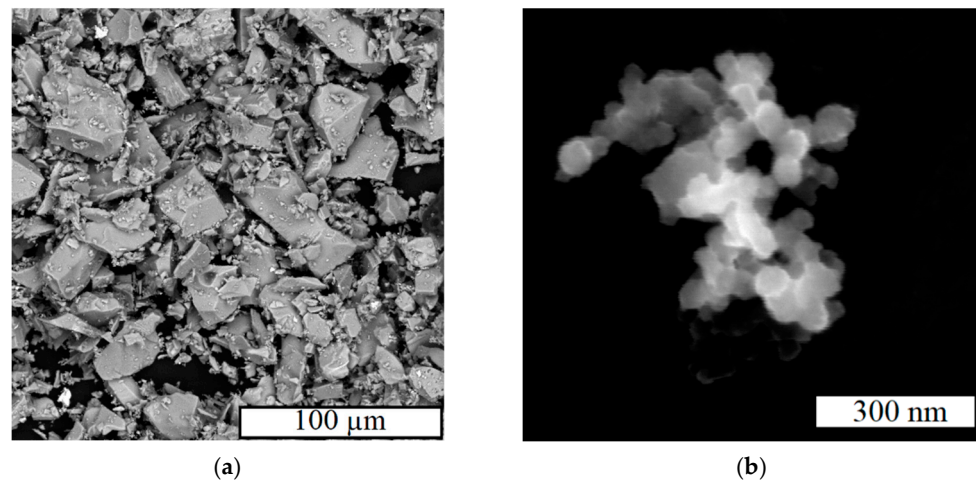


Figure 1. SEM images of the powders: micron-TiC (a), nano-TiC (b).

Table 1. Chemical compositions of TiC powders.

Powder	Ti, wt %	C, wt %	Fe, wt %	Mo, wt %
Micron-TiC	80.16	18.56	0.87	0.41
Nano-TiC	80.33	18.44	0.75	0.48

Mixtures of Inconel 718 and TiC particles were prepared by blending the powders in a gravitational mixer for 12 h.

The flowability of the powders was determined using ISO 4490, “Determination of flow rate by means of a calibrated funnel (Hall flowmeter)”. Apparent density measurements were made by pouring the powder into a funnel from which it flowed into a 25 cm^3 cup.

The particle size distribution of the powders was determined by laser diffraction on the Analysette 22 NanoTec plus (Fritsch GmbH, Idar-Oberstein, Germany) with a total measuring range of 0.01–2000 μm .

The microstructure of the powders and the obtained samples were studied using a Tescan Mira3 LMU (Brno, Czech Republic) scanning electron microscope (SEM) in secondary electron (SE) and backscattered electron (BSE) regimes and a Leica DMI5000 optical microscope. The etching of the samples was carried out in 25 mL of HNO_3 + 75 mL of HCL with a drop (approximately 0.03 mL) of hydrofluoric acid.

Samples were manufactured using the SLM280HL (SLM Solutions GmbH, Lübeck, Germany) selective laser melting system equipped with a YLR-Laser (wavelength of 1070 nm and focus size about 80 μm) under nitrogen atmosphere. The density of the obtained samples (blank and after HIP) was measured 6 times by the Archimedes method in water with a drop (approximately 0.03 mL) of surfactant.

The phase composition was analyzed with a Bruker D8 Advance (Billerica, MA, USA) X-ray diffractometer (XRD) using $\text{Cu-K}\alpha$ (1/4 1.5418 Å) irradiation. Three tests for each sample were performed.

Hot isostatic pressing (HIP) of the samples was processed at 1160 ± 5 °C and 130 MPa pressure for 3 h using argon gas. Heat treatment (H.T.) of the samples comprised annealing at 1060 ± 5 °C for 1 h, followed by air cooling and aging. Aging comprised heating to 760 ± 5 °C and holding for 10 h, then cooling to 650 ± 5 °C within 2 h and holding at 650 ± 5 °C for 8 h, followed by air cooling.

The hardness of the samples was determined using a Zwick/Roell Zhu (ZwickRoell GmbH & Co, Ulm, Germany) hardness tester using the Vickers method at 100 N. To determine the mean value, 10 tests were performed for cubical samples. Other mechanical properties of the samples (tensile strength, yield strength, relative elongation) were measured for hexagonal samples using a Zwick/Roell z050 (ZwickRoell GmbH & Co, Ulm, Germany) tensile testing machine at room temperature, 700 ± 10 °C and 1000 ± 10 °C.

Phoenix v|tome|x m300 Industrial High-Resolution Computed Tomography System (Waygate Technologies, Wunstorf, Germany) was used for X-ray microtomography analysis (xCT) for the samples after HIP and H.T.

3. Results

3.1. Initial Powders

Initial powders of Inconel 718 (Inc 718) and its mixtures with micron-sized TiC (Inc 718 + 1% micron-TiC) and nano-sized TiC (Inc 718 + 1% nano-TiC) were studied. The technological properties of the powders are presented in Table 2. All the powders can flow through the Hall flowmeter funnel freely, indicating their spreading ability during the SLM process. The decreasing apparent density of the powder with micron-TiC is connected to the morphology of the micron-TiC particles (Figure 2b). The SEM images of the powders (Figure 2) demonstrate that Inc 718 particles can be characterized as rounded and spherical-shaped, and micron-TiC particles can be described as polyhedral. Micron-TiC particles are evenly distributed in the Inc 718 powder, and nano-TiC particles are concentrated at the Inc 718 particle surface (Figure 2d).

Table 2. Technological properties of the powders.

Powder	Flow Rate, s/50 g	Apparent Density, g/cm ³
Inc 718	12.0 ± 0.2	4.67 ± 0.12
Inc 718 + 1% micron-TiC	13.6 ± 0.2	4.28 ± 0.07
Inc 718 + 1% nano-TiC	13.4 ± 0.2	4.64 ± 0.10

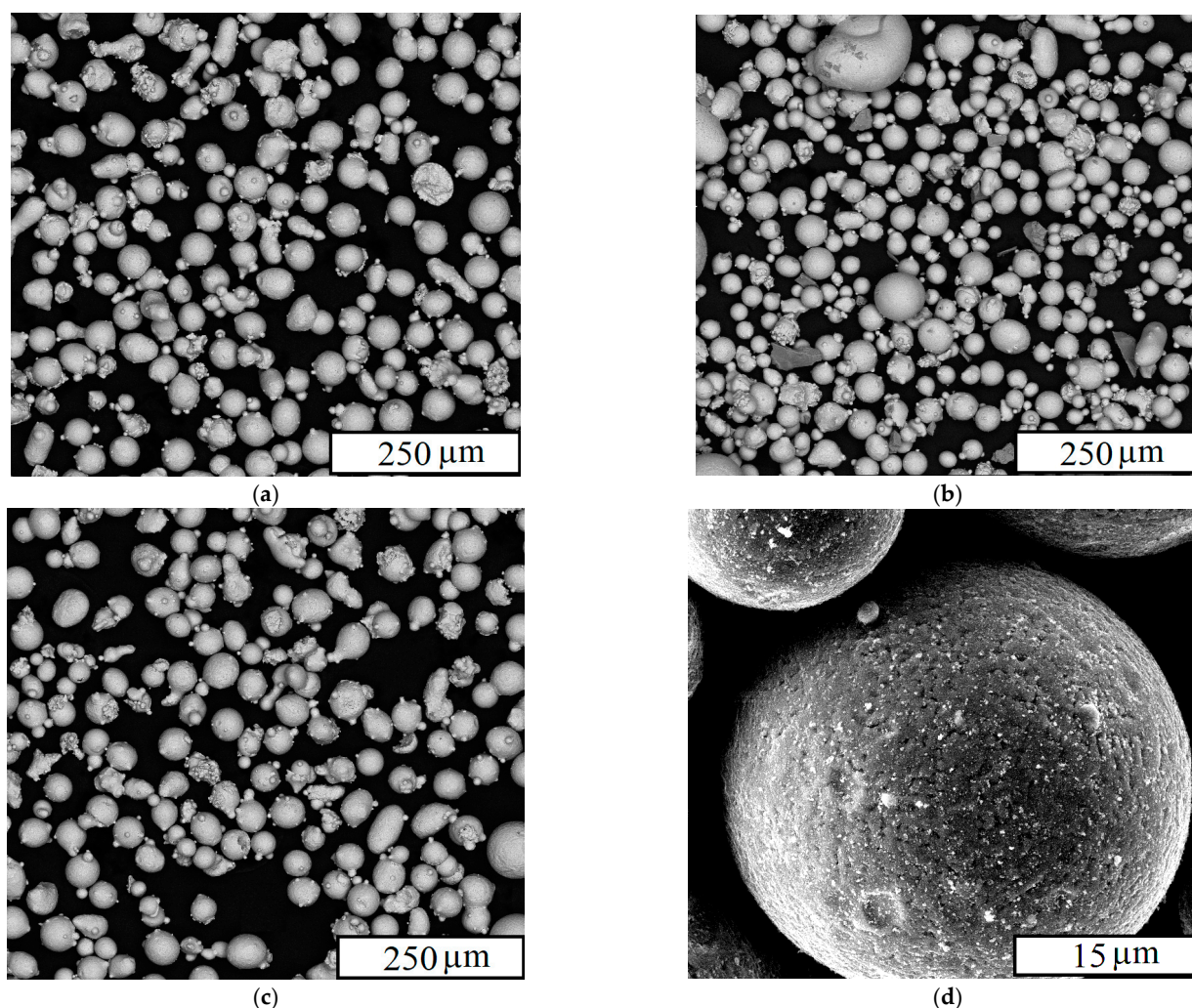


Figure 2. SEM images of the powders: Inc 718 (a) (BSE), Inc 718 + 1% micron-TiC (b) (BSE), Inc 718 + 1% nano-TiC (c) (BSE), nano-TiC particles on the Inconel particle surface (d) (SE).

Powders' particle size distribution data are presented in Table 3. All the powders' particle sizes are Gaussian-distributed, except powder containing nano-TiC, whose distribution curve contains a “hump” in a nano-sized area. The mean values of the powders' particle size are 38.9 μm , 39.8 μm and 39.7 μm for Inc 718 and its mixtures with micron-TiC and nano-TiC, respectively. Such particle size characteristics are suitable for SLM and typical in the practice of using this technology [8,9].

Table 3. Particle size distribution of the powders.

Powder	d_{10} , μm	d_{50} , μm	d_{90} , μm
Inc 718	21.4 ± 1.1	38.9 ± 1.1	66.4 ± 1.1
Inc 718 + 1% micron-TiC	21.6 ± 0.9	39.8 ± 0.9	68.3 ± 0.9
Inc 718 + 1% nano-TiC	20.5 ± 1.2	39.7 ± 1.2	67.5 ± 1.2

3.2. SLM Samples

Seventeen SLM samples of each powder were successfully manufactured in a nitrogen atmosphere. Eleven samples had a cubical geometry, and six samples had a form of hexagonal prism. Parameters applied for SLM fabrication were identical for all the samples and are presented in Table 4.

Table 4. Parameters applied for SLM fabrication.

Laser Power (W)	Laser Scanning Speed (mm/s)	Hatch Distance (mm)	Layer Thickness (mm)
250	700	0.12	0.05

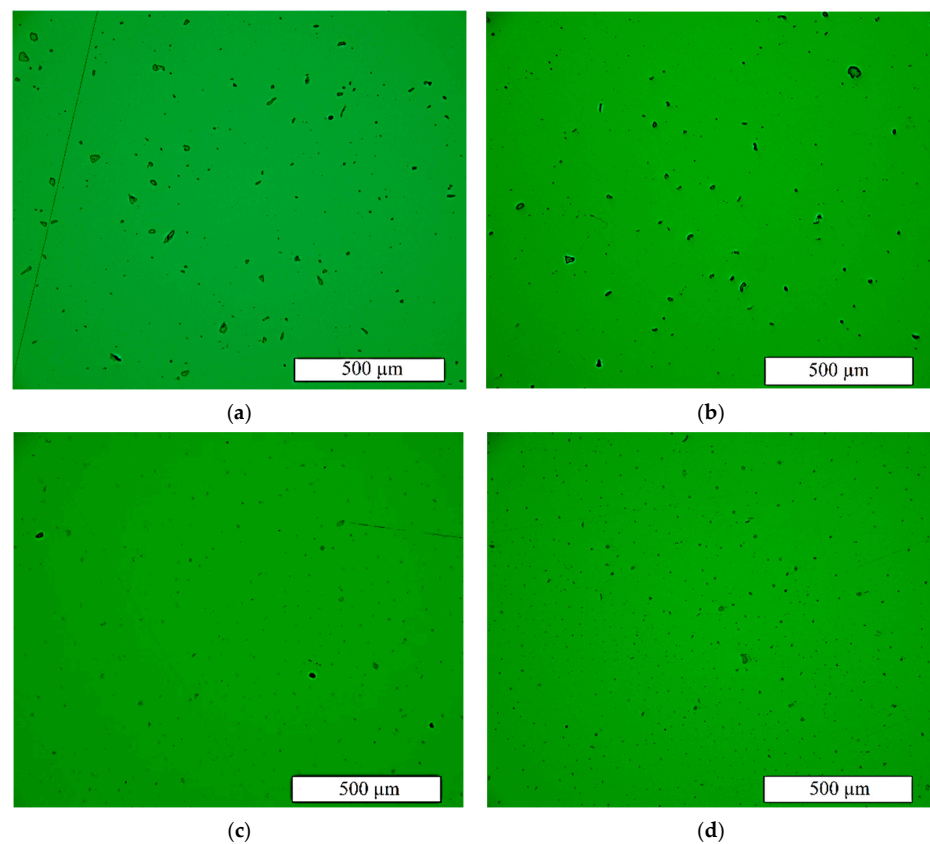
It should be noted that manufacturing of the samples by the SLM process was carried out in a horizontal direction. Horizontally grown specimens, in contrast to vertically grown ones, have higher strength values and lower elongation [31,32].

The density of the sample data is presented in Table 5. The obtained values show that hot isostatic pressing slightly increased the density of the samples obtained with mixed powders and had no significant effect on Inc 718 because of single amounts of small pores in blank samples, which indicates that the SLM parameters used are acceptable for this composition.

Table 5. Density of the fabricated samples.

Sample	Density, g/cm ³
Inc 718	8.19 ± 0.02
Inc 718 + micron-TiC	8.13 ± 0.01
Inc 718 + nano-TiC	8.18 ± 0.01
Inc 718 HIP + H.T.	8.19 ± 0.02
Inc 718 + micron-TiC HIP + H.T.	8.16 ± 0.02
Inc 718 + nano-TiC HIP + H.T.	8.19 ± 0.01

The distribution of the TiC particles in the Inc 718 matrix was examined by an optical microscope (Figure 3).

**Figure 3.** Optical microscope images of the TiC particles in SLM samples: (a) Inc 718 + micron-TiC, (b) Inc 718 + micron-TiC after HIP + H.T., (c) Inc 718 + nano-TiC, (d) Inc 718 + nano-TiC after HIP + H.T.

Micron-TiC particles' distribution can be characterized as even, which is favorable for strengthening, but the same cannot be said about nano-TiC particles' distribution. It is clear that nano-TiC particles are at least partially agglomerated, which means that the effect of the nano-sized TiC evenly distributed in the Inc 718 matrix cannot be fully observed. A similar situation was observed in another experiment [20].

Figure 4 shows the results of xCT with distribution of the TiC particles in the Inc 718 matrix.

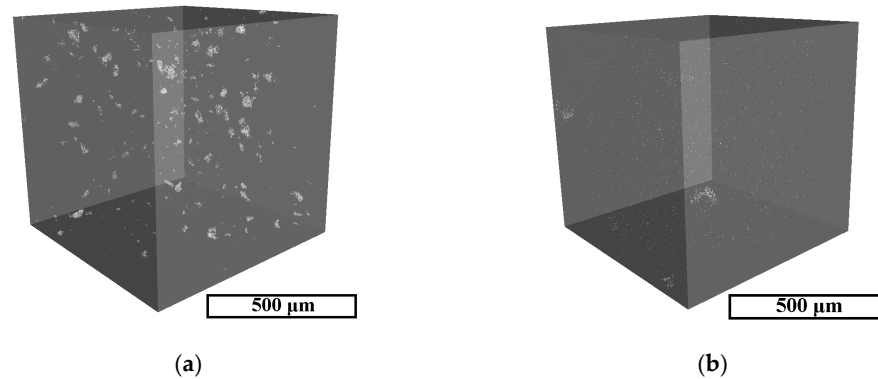


Figure 4. Images of xCT reconstructions of volumes with distribution of the TiC particles in SLM samples: (a) Inc 718 + micron-TiC, (b) Inc 718 + nano-TiC.

The results of the xCT investigation demonstrate a uniform distribution of micron-sized particles of TiC, as well as the presence of agglomerates in the case of a sample with nano-sized particles of TiC.

The phase composition of the processed (HIP + H.T.) samples was studied with X-ray diffraction (Figure 5). All the tests for each sample came back with the same results. Obtained data show that the samples contain the following phases: MC (metal carbide), TiC (JCPDS Card No. 65-8805) and γ/γ'' -phase (JCPDS Card No. 47-1417 and 49-1427).

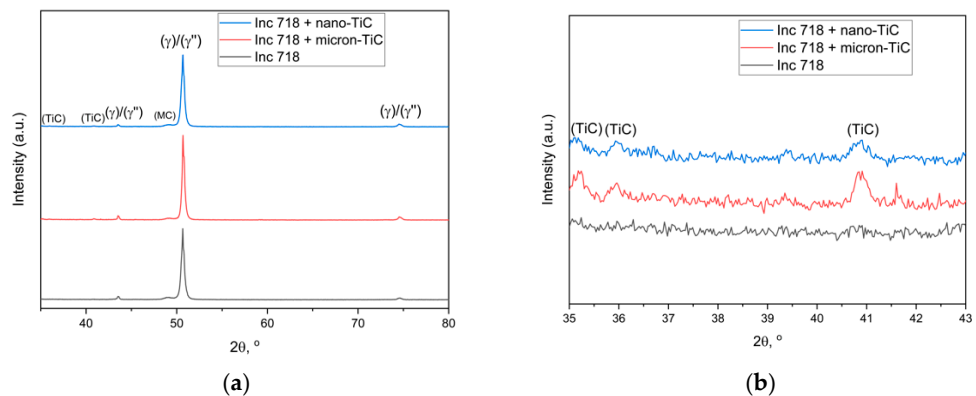


Figure 5. X-ray diffraction patterns of the processed (HIP + H.T.) samples (a); enlarged part of the graph (b).

The small size of the peaks connected with TiC can be explained by its small mass fraction (1%). The γ'' -phase is coherent to the γ -phase and its reflexes are located at the same angles as γ . Titan carbide (TiC) cannot be included in MC-phase notation because peaks related to TiC can only be observed in samples containing TiC, which cannot be said about the peak marked as MC.

The microstructure of the samples after treatment was investigated with SEM (Figure 6). Carbide MC phases (white) that precipitated after aging with a mean size of 0.5 μm are located mainly on grain boundaries in all three samples, and their distribution can be considered as even in all the samples. Some of the nano-TiC particles are not agglomerated (Figure 6d), which means that their strengthening effects can be observed.

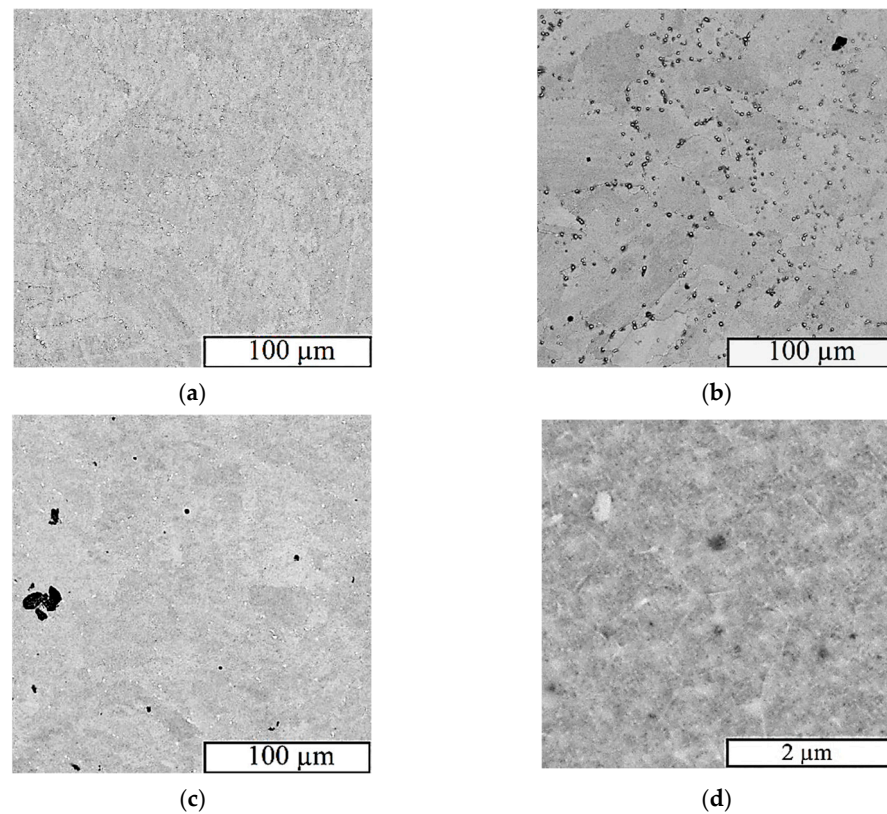


Figure 6. Microstructure of the processed samples (backscattered electron, SEM): (a) Inc 718, (b) Inc 718 + micron-TiC, (c) Inc 718 + nano-TiC, (d) nano-TiC particles (dark regions) in Inc 718 matrix.

Figure 7 shows that the metal carbide MC phase locates at the γ -phase cell grain boundaries, and the γ'' -phase is evenly distributed in cells in all processed samples. An assessment of the size of cells and phases across the entire plane of the specimen does not allow us to conclude that there is an influence of TiC size on structural components' size in processed samples with 1% TiC. This means that all influences on the mechanical properties exerted by TiC should be related to Orowan strengthening only and not to the Hall–Petch mechanism. It seems that undesired phases (Delta, Laves, etc.) are absent in all samples, which correlates to the X-ray diffraction data.

Microhardness data are presented in Table 6. In general, the addition of 1% TiC in the Inc 718 matrix results in slightly increased hardness: the sample with micron-TiC demonstrated a 6% increase in hardness, and the sample with nano-TiC was 5% harder. Post-processing hot isostatic pressing and heat treatment led to hardening of the Inc 718 sample by 18%, and for samples with micron-TiC and nano-TiC, the hardness values increased by 22% and 20%, respectively. Micron- and nano-TiC particles had approximately equal efficiency in increasing the hardness of Inc 718, which may be related to the partial agglomeration of the nano-TiC particles.

Table 6. Hardness of the samples (HV₁₀).

Sample	Hardness
Inc 718	372 ± 14
Inc 718 + micron-TiC	395 ± 9
Inc 718 + nano-TiC	391 ± 8
Inc 718 HIP + H.T.	440 ± 10
Inc 718 + micron-TiC HIP + H.T.	483 ± 9
Inc 718 + nano-TiC HIP + H.T.	472 ± 12

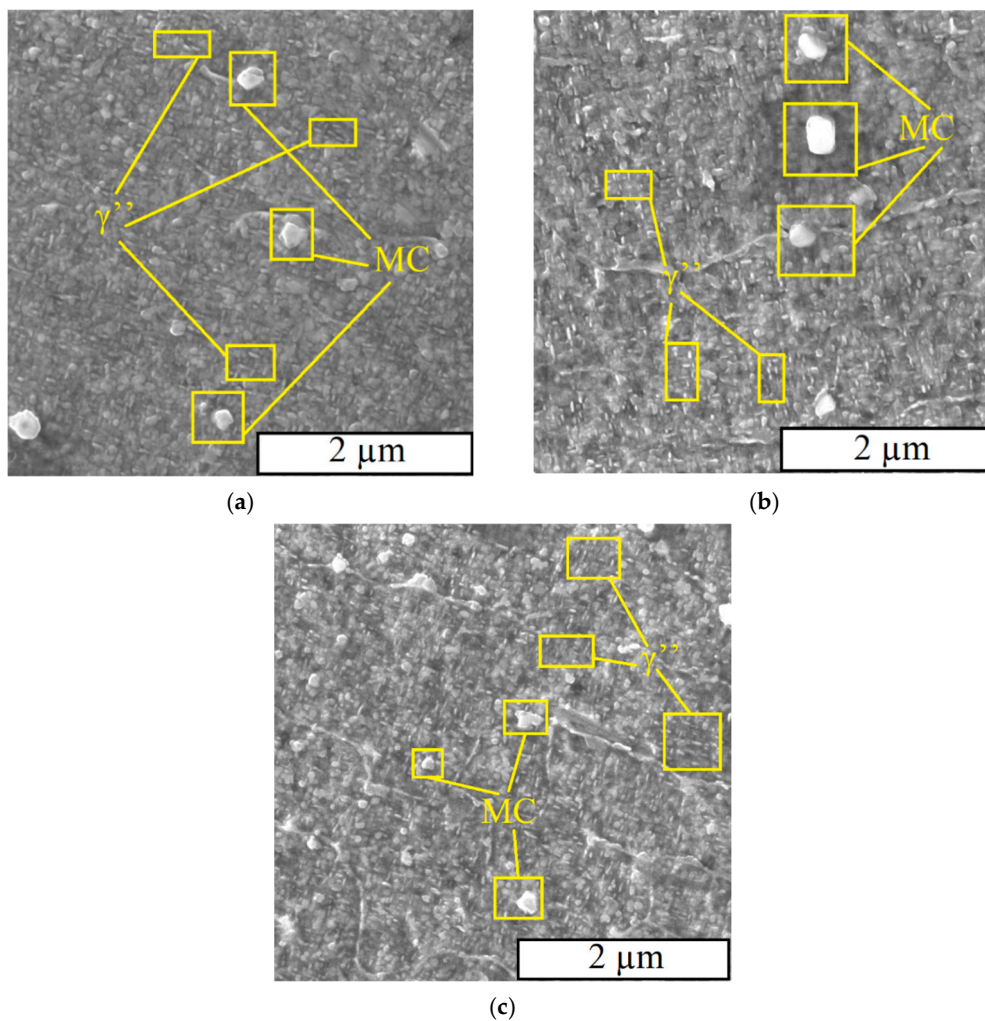


Figure 7. Microstructure of the processed samples with marked phases (secondary electron, SEM): (a) Inc 718, (b) Inc 718 + micron-TiC, (c) Inc 718 + nano-TiC.

The results of tensile tests of the post-processed samples at room temperature, 700 °C and 1000 °C are presented in Table 7, and engineering stress–strain curves are presented in Figure 8.

Table 7. Mechanical properties of post-processed SLM samples at different temperatures.

Sample	Test Temperature, °C	YS, MPa	UTS, MPa	δ , %
Inc 718 HIP + H.T.	25	1180 ± 8	1400 ± 7	12.4
Inc 718 + micron-TiC HIP + H.T.	25	1220 ± 4	1450 ± 13	11.5
Inc 718 + nano-TiC HIP + H.T.	25	1260 ± 3	1490 ± 9	9.8
Inc 718 HIP + H.T.	700	912 ± 2	938 ± 7	7.3
Inc 718 + micron-TiC HIP + H.T.	700	958 ± 7	985 ± 8	5.9
Inc 718 + nano-TiC HIP + H.T.	700	985 ± 6	1008 ± 5	5.3
Inc 718 HIP + H.T.	1000	95 ± 5	101 ± 1	43.2
Inc 718 + micron-TiC HIP + H.T.	1000	103 ± 1	105 ± 1	42.6
Inc 718 + nano-TiC HIP + H.T.	1000	97 ± 1	102 ± 1	39.2

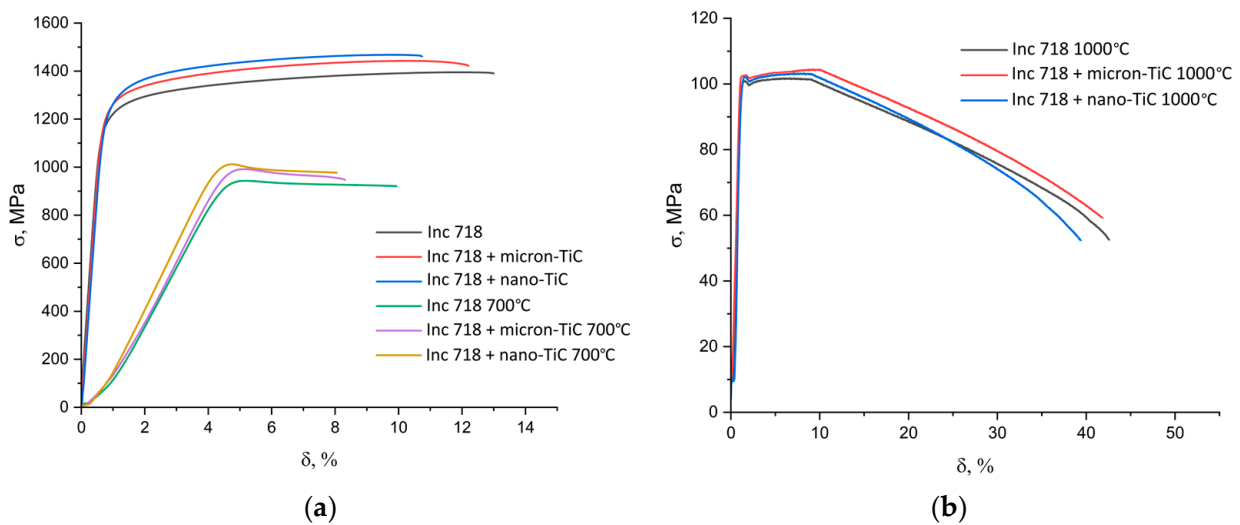


Figure 8. Engineering stress–strain curves for post-processed samples tested at room temperature and 700 °C (a) and 1000 °C (b).

A monotonous increase in mechanical strength and a decrease in relative elongation were observed with the addition of TiC particles of decreasing size: the addition of 1% micron- and nano-TiC increased yield and ultimate tensile strength by approximately 3.5% and 6.5%, respectively, at room temperature, and by 5% and 7%, respectively, at 700 °C, and decreased relative elongation by 8% and 26%, respectively, at room temperature, and by 24% and 38%, respectively, at 700 °C. This effect is connected to the Orowan strengthening mechanism based on dislocation bending between particles: decreasing the particle size from micron to nano sizes yields a stronger material because of dislocation movement impediment (which also decreases relative elongation). Mechanical tests showed that some positive effects of TiC addition can be achieved at room temperature and 700 °C, and moreover, increasing strength is slightly higher at 700 °C. Tests at 1000 °C showed that the addition of a small percentage of TiC particles cannot provide a decent level of mechanical properties at temperatures far exceeding the maximal working temperature (700 °C for Inc 718 alloy [33]).

4. Conclusions

1. Selective laser melting of Inc718/TiC composites (without a difference using micron-sized or nano-sized 1% TiC) and subsequent hot isostatic pressing and heat treatment have no influence on the final grain and precipitation sizes of the matrix material.
2. The addition of 1% micron-TiC or 1% nano-TiC particles has similar efficiency in increasing the hardness of the composite material; the effect amounts to approximately 5% for as-built material and about 20% for material after hot isostatic pressing and heat treatment.
3. The addition of 1% micron- and nano-TiC and the use of hot isostatic pressing with heat treatment increases the mechanical strength of selective laser-melted Inconel 718 by approximately 3.5% and 6.5%, respectively, at room temperature, and by 5% and 7%, respectively, at 700 °C. Furthermore, it decreases relative elongation by 8% and 26%, respectively, at room temperature, and by 24% and 38%, respectively, at 700 °C. The used percentage of TiC particles cannot provide an adequate level of mechanical properties at 1000 °C.

Author Contributions: Conceptualization, V.S.; methodology, V.S. and E.B.; formal analysis, D.E.; investigation, E.B. and D.E.; resources, V.S. and A.P.; data curation, D.E. and E.B.; writing—original draft preparation, D.E. and V.S.; writing—review and editing, D.E. and V.S.; visualization, D.E.; project administration, V.S. and E.B.; funding acquisition, V.S. and A.P. All authors have read and agreed to the published version of the manuscript.

Funding: The research was funded by the Ministry of Science and Higher Education of the Russian Federation: “Agreement on the grant in the form of subsidies from the federal budget for the implementation of state support for the creation and development of world-class scientific centers, those are performing research and development on the priorities of scientific and technological development”, dated 20 April 2022, no. 075-15-2022-311.

Data Availability Statement: Not applicable.

Acknowledgments: The authors thank the OSTEC-SMT company for the X-ray computed tomography analysis.

Conflicts of Interest: The authors declare no conflict of interest.

References

1. Song, K.H.; Nakata, K. Microstructure and mechanical properties of friction stir welded inconel 718 alloy. *Ceram. Trans.* **2010**, *219*, 391–396. [[CrossRef](#)]
2. Yilbas, B.S.; Ali, H.; Al-Aqeeli, N.; Karatas, C. Laser treatment of Inconel 718 alloy and surface characteristics. *Opt. Laser Technol.* **2016**, *78*, 153–158. [[CrossRef](#)]
3. Chang, S.H. In situ TEM observation of γ' , γ'' and δ precipitations on Inconel 718 superalloy through HIP treatment. *J. Alloys Compd.* **2009**, *486*, 716–721. [[CrossRef](#)]
4. Popovich, A.A.; Sufiiarov, V.S.; Borisov, E.V.; Polozov, I.A.; Masaylo, D.V. Design and manufacturing of tailored microstructure with selective laser melting. *Mater. Phys. Mech.* **2018**, *38*, 1–10. [[CrossRef](#)]
5. Sufiiarov, V.S.; Borisov, E.V.; Polozov, I.A.; Masailo, D.V. Control of structure formation in selective laser melting process. *Tsvetnye Met.* **2018**, *7*, 68–74. [[CrossRef](#)]
6. Sufiiarov, V.S.; Popovich, A.A.; Borisov, E.V.; Polozov, I.A. Evolution of structure and properties of heatresistant nickel alloy after selective laser melting, hot isostatic pressing and heat treatment. *Tsvetnye Met.* **2017**, *1*, 77–82. [[CrossRef](#)]
7. Gu, D. *Laser Additive Manufacturing of High-Performance Materials*; Springer: Berlin/Heidelberg, Germany, 2015; ISBN 9783662460894.
8. Raghavan, S.; Zhang, B.; Wang, P.; Sun, C.-N.; Nai, M.L.S.; Li, T.; Wei, J. Effect of different heat treatments on the microstructure and mechanical properties in selective laser melted INCONEL 718 alloy. *Mater. Manuf. Process.* **2017**, *32*, 1588–1595. [[CrossRef](#)]
9. Casalino, G.; Campanelli, S.L.; Contuzzi, N.; Ludovico, A.D. Experimental investigation and statistical optimisation of the selective laser melting process of a maraging steel. *Opt. Laser Technol.* **2015**, *65*, 151–158. [[CrossRef](#)]
10. Sun, J.; Yang, Y.; Wang, D. Parametric optimization of selective laser melting for forming Ti6Al4V samples by Taguchi method. *Opt. Laser Technol.* **2013**, *49*, 118–124. [[CrossRef](#)]
11. Calandri, M.; Manfredi, D.; Calignano, F.; Ambrosio, E.P.; Biamino, S.; Lupoi, R.; Ugues, D. Solution Treatment Study of Inconel 718 Produced by SLM Additive Technique in View of the Oxidation Resistance. *Adv. Eng. Mater.* **2018**, *20*, 1800351. [[CrossRef](#)]
12. Sufiiarov, V.S.; Popovich, A.A.; Borisov, E.V.; Polozov, I.A. Layer thickness influence on the inconel 718 alloy microstructure and properties under selective laser melting. *Tsvetnye Met.* **2016**, *1*, 81–86. [[CrossRef](#)]
13. Thomas, A.; El-Wahabi, M.; Cabrera, J.M.; Prado, J.M. High temperature deformation of Inconel 718. *J. Mater. Process. Technol.* **2006**, *177*, 469–472. [[CrossRef](#)]
14. Slama, C.; Abdellaoui, M. Structural characterization of the aged Inconel 718. *J. Alloys Compd.* **2000**, *306*, 277–284. [[CrossRef](#)]
15. Cozar, R.; Pineau, A. Morphology of γ' and γ'' precipitates and thermal stability of inconel 718 type alloys. *Metall. Trans.* **1973**, *4*, 47–59. [[CrossRef](#)]
16. Sundararaman, M.; Mukhopadhyay, P.; Banerjee, S. Precipitation and Room Temperature Deformation Behaviour of Inconel 718. *Superalloys* **2012**, *718*, 419–440. [[CrossRef](#)]
17. Sundararaman, M.; Mukhopadhyay, P.; Banerjee, S. Precipitation of the δ -Ni₃Nb phase in two nickel base superalloys. *Metall. Trans. A* **1988**, *19*, 453–465. [[CrossRef](#)]
18. Hong, C.; Gu, D.; Dai, D.; Gasser, A.; Weisheit, A.; Kelbassa, I.; Zhong, M.; Poprawe, R. Laser metal deposition of TiC/Inconel 718 composites with tailored interfacial microstructures. *Opt. Laser Technol.* **2013**, *54*, 98–109. [[CrossRef](#)]
19. Kong, D.; Dong, C.; Ni, X.; Zhang, L.; Man, C.; Zhu, G.; Yao, J.; Wang, L.; Cheng, X.; Li, X. Effect of TiC content on the mechanical and corrosion properties of Inconel 718 alloy fabricated by a high-throughput dual-feed laser metal deposition system. *J. Alloys Compd.* **2019**, *803*, 637–648. [[CrossRef](#)]
20. Zhang, H.; Gu, D.; Xi, L.; Zhang, H.; Xia, M.; Ma, C. Anisotropic corrosion resistance of TiC reinforced Ni-based composites fabricated by selective laser melting. *J. Mater. Sci. Technol.* **2019**, *35*, 1128–1136. [[CrossRef](#)]

21. Xia, M.; Gu, D.; Ma, C.; Chen, H.; Zhang, H. Microstructure evolution, mechanical response and underlying thermodynamic mechanism of multi-phase strengthening WC/Inconel 718 composites using selective laser melting. *J. Alloys Compd.* **2018**, *747*, 684–695. [[CrossRef](#)]
22. Kim, S.H.; Shin, G.H.; Kim, B.K.; Kim, K.T.; Yang, D.Y.; Aranas, C.; Choi, J.P.; Yu, J.H. Thermo-mechanical improvement of Inconel 718 using ex situ boron nitride-reinforced composites processed by laser powder bed fusion. *Sci. Rep.* **2017**, *7*, 1–13. [[CrossRef](#)] [[PubMed](#)]
23. Tang, B.; Tan, Y.; Zhang, Z.; Xu, T.; Sun, Z.; Li, X. Effects of process parameters on geometrical characteristics, microstructure and tribological properties of TiB₂ reinforced inconel 718 alloy composite coatings by laser cladding. *Coatings* **2020**, *10*, 76. [[CrossRef](#)]
24. Bonatti, R.S.; Siqueira, R.R.; Padilha, G.S.; Bortolozzo, A.D.; Osório, W.R. Distinct Alp/Sip composites affecting its densification and mechanical behavior. *J. Alloys Compd.* **2018**, *757*, 434–447. [[CrossRef](#)]
25. Ma, K.; Lavernia, E.J.; Schoenung, J.M. Particulate reinforced aluminum alloy matrix composites—A review on the effect of microconstituents. *Rev. Adv. Mater. Sci.* **2017**, *48*, 91–104.
26. Bouvard, D. Densification behaviour of mixtures of hard and soft powders under pressure. *Powder Technol.* **2000**, *111*, 231–239. [[CrossRef](#)]
27. Meyer, Y.A.; Bonatti, R.S.; Bortolozzo, A.D.; Osório, W.R. Electrochemical behavior and compressive strength of Al-Cu/xCu composites in NaCl solution. *J. Solid State Electrochem.* **2021**, *25*, 1303–1317. [[CrossRef](#)]
28. Sahoo, C.K.; Masanta, M. Microstructure and mechanical properties of TiC-Ni coating on AISI304 steel produced by TIG cladding process. *J. Mater. Process. Technol.* **2017**, *240*, 126–137. [[CrossRef](#)]
29. Wang, Y.; Shi, J.; Wang, Y. Reinforcing inconel 718 superalloy by nano-TiC particles in selective laser melting. In Proceedings of the ASME 2015 International Manufacturing Science and Engineering Conference, MSEC 2015, College Station, TX, USA, 18–20 June 2015; American Society of Mechanical Engineers: New York, NY, USA, 2015; Volume 2, p. V002T05A018.
30. Wang, Y.; Shi, J.; Lu, S.; Wang, Y. Solution and aging treatments of Inconel 718/TiC nanocomposite from selective laser melting. In Proceedings of the ASME 2016 11th International Manufacturing Science and Engineering Conference, MSEC 2016, Blacksburg, VA, USA, 27 June–1 July 2016; American Society of Mechanical Engineers: New York, NY, USA, 2016; Volume 3, p. V003T08A004.
31. Popovich, A.A.; Sufiiarov, V.S.; Borisov, E.V.; Polozov, I.A.; Masaylo, D.V.; Grigoriev, A.V. Anisotropy of mechanical properties of products manufactured using selective laser melting of powdered materials. *Russ. J. Non-Ferrous Met.* **2017**, *58*, 389–395. [[CrossRef](#)]
32. Deng, D.; Peng, R.L.; Brodin, H.; Moverare, J. Microstructure and mechanical properties of Inconel 718 produced by selective laser melting: Sample orientation dependence and effects of post heat treatments. *Mater. Sci. Eng. A* **2018**, *713*, 294–306. [[CrossRef](#)]
33. Special Metals Corporation, Inconel[®] Alloy 718. Available online: http://www.specialmetals.com/assets/smc/documents/inconel_alloy_718.pdf (accessed on 12 September 2022).